Two-Equation Turbulence Models for Prediction of Heat Transfer on a Transonic Turbine Blade

Vijay K. Garg and Ali A. Ameri
AYT Corporation, Brook Park, Ohio

Since its founding, NASA has been dedicated to the advancement of aeronautics and space science. The NASA Scientific and Technical Information (STI) Program Office plays a key part in helping NASA maintain this important role.

The NASA STI Program Office is operated by Langley Research Center, the Lead Center for NASA's scientific and technical information. The NASA STI Program Office provides access to the NASA STI Database, the largest collection of aeronautical and space science STI in the world. The Program Office is also NASA's institutional mechanism for disseminating the results of its research and development activities. These results are published by NASA in the NASA STI Report Series, which includes the following report types:

- TECHNICAL PUBLICATION. Reports of completed research or a major significant phase of research that present the results of NASA programs and include extensive data or theoretical analysis. Includes compilations of significant scientific and technical data and information deemed to be of continuing reference value. NASA's counterpart of peer-reviewed formal professional papers but has less stringent limitations on manuscript length and extent of graphic presentations.

- TECHNICAL MEMORANDUM. Scientific and technical findings that are preliminary or of specialized interest, e.g., quick release reports, working papers, and bibliographies that contain minimal annotation. Does not contain extensive analysis.

- CONTRACTOR REPORT. Scientific and technical findings by NASA-sponsored contractors and grantees.

- CONFERENCE PUBLICATION. Collected papers from scientific and technical conferences, symposia, seminars, or other meetings sponsored or cosponsored by NASA.

- SPECIAL PUBLICATION. Scientific, technical, or historical information from NASA programs, projects, and missions, often concerned with subjects having substantial public interest.

- TECHNICAL TRANSLATION. English-language translations of foreign scientific and technical material pertinent to NASA's mission.

Specialized services that complement the STI Program Office's diverse offerings include creating custom thesauri, building customized data bases, organizing and publishing research results . . . even providing videos.

For more information about the NASA STI Program Office, see the following:

- Access the NASA STI Program Home Page at *http://www.sti.nasa.gov*

- E-mail your question via the Internet to help@sti.nasa.gov

- Fax your question to the NASA Access Help Desk at 301–621–0134

- Telephone the NASA Access Help Desk at 301–621–0390

- Write to:
  NASA Access Help Desk
  NASA Center for AeroSpace Information
  7121 Standard Drive
  Hanover, MD 21076

2001–GT–0165

Two-Equation Turbulence Models for Prediction of Heat Transfer on a Transonic Turbine Blade

Vijay K. Garg and Ali A. Ameri
AYT Corporation, Brook Park, Ohio

Acknowledgments

TWO-EQUATION TURBULENCE MODELS FOR PREDICTION OF HEAT TRANSFER ON A TRANSONIC TURBINE BLADE

Vijay K. Garg and Ali A. Ameri
AYT Corporation
2001 Aerospace Parkway
Brook Park, Ohio 44142

ABSTRACT

Two versions of the two-equation k-ω model and a shear stress transport (SST) model are used in a three-dimensional, multi-block, Navier-Stokes code to compare the detailed heat transfer measurements on a transonic turbine blade. It is found that the SST model resolves the passage vortex better on the suction side of the blade, thus yielding a better comparison with the experimental data than either of the k-ω models. However, the comparison is still deficient on the suction side of the blade. Use of the SST model does require the computation of distance from a wall, which for a multi-block grid, such as in the present case, can be complicated. However, a relatively easy fix for this problem was devised. Also addressed are issues such as (1) computation of the production term in the turbulence equations for aerodynamic applications, and (2) the relation between the computational and experimental values for the turbulence length scale, and its influence on the passage vortex on the suction side of the turbine blade.

NOMENCLATURE

C_p specific heat at constant pressure
F_1, F_2 constants defined in Eqs. (7) and (10)
k turbulence kinetic energy; also thermal conductivity in Eq. (20)
ℓ turbulence length scale
M Mach number
Pr Prandtl number
r recovery factor = $Pr^{1/3}$ (for turbulent flow)
Re Reynolds number based on the blade axial chord and U_{in}
R_{ii} auto-correlation tensor for velocity
s distance from the leading edge along the pressure or suction surface
S strain rate
St Stanton number defined in Eq. (20)
T temperature
Tu turbulence intensity
u velocity
U magnitude of velocity

v^* shear velocity
x,y,z Cartesian coordinate system with origin at the geometric stagnation point, and z in the spanwise direction
y^+ distance in wall coordinates (= yv^*/v)
α thermal diffusivity
α_1 constant in Eqs. (8) and (9)
β, β^* constants given in Eqs. (8) and (12)
Δy distance (from the wall) of the first point off the wall
ε turbulence dissipation rate
γ constant given in Eqs. (8) and (12); also ratio of specific heats in Eq. (21)
κ von Karman constant given in Eq. (8)
μ viscosity
v kinematic viscosity
ρ density
σ constants given in Eqs. (8) and (12)
τ shear stress
ω specific turbulence dissipation rate (= ε/k)
Ω absolute value of vorticity

Subscripts
aw   adiabatic wall value
ef   effective value
ex   value at exit
exp   experimental value
in   value at inlet
is   isentropic value
ℓ laminar value
o   stagnation value
t   turbulent value
w   value at wall

INTRODUCTION

Accurate prediction of turbine blade heat transfer, so crucial to the efficient design of blade cooling schemes, still remains a challenging task despite a lot of work in this area. The main cause for the lack of

agreement with experimental data in such predictions is usually cited to be the turbulence modeling. This is due to a variety of flow and heat transfer phenomena which are encountered in turbine passages. Stagnation flow heat transfer, heat transfer in the presence of steep pressure gradients both favorable and adverse, free stream turbulence, high Mach number and three-dimensional effects are only some of the items in a long list of phenomena present in these passages.

Well documented data sets exist which test the capabilities of numerical schemes for the prediction of blade heat transfer. The NASA Glenn transonic blade (Giel et al., 1999) is an example of such a challenging test case that will be examined in this work. It is a data set for a rotor cascade with a large turning angle. The experimental heat transfer measurements are available for the blade at three spanwise locations for varying exit Mach number, Reynolds number, inlet turbulence intensity as well as the inlet boundary layer thickness to the cascade. Some of the cases are highly three-dimensional and pose a severe challenge to the predictive ability of any numerical scheme.

As the direct numerical simulation of such flows are not anticipated to become routine for many more years, turbulence modeling seems to remain the only option. By far the most popular turbulence models utilized today for flow and heat transfer calculations are the low-Reynolds number two-equation eddy viscosity models. The k-ε and k-ω are the most utilized models. These models often offer a good balance between complexity and accuracy. The ability to mimic transition to turbulence which often is present on turbine blades and the ability to integrate to the walls are other reasons for their popularity. These models have been applied to a variety of experimentally measured cases and their accuracy assessed, yet they do not offer good comparisons consistently. There are also questions regarding the modeling of the stagnation heat transfer and the free-stream turbulence, and the best manner to specify them as boundary conditions.

It was found during the course of this work that the low-Reynolds number version of the k-ω turbulence model adopted as the basic model in the Glenn-HT code was inadequate in predicting the blade surface heat transfer for this case. Thus, use of other eddy viscosity models was explored. Our preference for the k-ω model stems from its robustness and absence of the distance to the wall in its formulation, which makes it attractive for a multi-block code. The models tested other than the original k-ω model (Wilcox, 1988) were the 1998 k-ω model (Wilcox, 1998) and Menter's SST model (1994). Menter's SST model among these performed the best. This model was devised by combining good near-wall behavior of the Wilcox's k-ω model, and the k-ε model (Jones and Launder, 1973) away from the walls. Menter reports much improved agreement with experiments (Menter, 1994, 1996) for velocity profiles, pressure distributions and skin friction distributions for a variety of test cases. The SST model does require the computation of distance to the wall in its formulation, the implementation of which is discussed later in the paper.

The computation of the leading edge heat transfer also requires special attention. It has been reported by Menter (1994) and others that the use of eddy viscosity models causes overprediction of the turbulence production term. This in turn leads to overprediction of the leading edge heat transfer. Two "fixes" for this have been suggested

by Menter (1992) and by Kato and Launder (1993). These have been tested in this work.

The experiment under consideration provides both the inlet turbulence intensity and length scale in the form of an integral length scale. As many experiments do not provide the length scale, the CFD practitioner feels free to choose a value, often one that best fits the experimental data (Moore and Moore, 1999). Moss and Oldfield (1992) studied the effect of free-stream turbulence scale on heat transfer over a flat plate and concluded that the heat transfer coefficient cannot be predicted accurately using turbulence level alone, but a reasonable prediction can be made using the turbulence level and the integral scale even for highly anisotropic turbulence at high intensities. Van Fossen et al. (1995) also found that the turbulence length scale affects the stagnation region heat transfer. Even when the experimental length scale is known, such as in the present case, the computational value may not be the same. This is described later on. For flow over a blade, the turbulence length scale also affects the passage vortex on the suction side of the blade - an essentially three-dimensional phenomenon. It is therefore essential to use a correct value for the turbulence length scale.

In this paper following the introduction, equations for the turbulence models considered are presented. Next the computation of production term in the turbulence model equations is discussed, and the relation between the experimental and computational value of the turbulence length scale is defined. Their effects on sample calculations are then examined. Subsequently the results of the calculations with the various models are presented and compared with the experimental data.

ANALYSIS

The numerical simulation has been performed using the NASA Glenn Research Center General Multi-Block Navier-Stokes Convective Heat Transfer code, Glenn-HT. Briefly, the code, formerly known as TRAF3D.MB (Steinthorsson et al., 1997), is an explicit, multigrid, cell-centered, finite volume code with a k-ω turbulence model without any wall functions. This is a general purpose flow solver designed for simulations of flows in complicated geometries. The Navier-Stokes equations in a rotating Cartesian coordinate system are mapped onto a general body-fitted coordinate system using standard techniques. The multistage Runge-Kutta scheme developed by Jameson et al. (1981) is used to advance the flow solution in time from an initial approximation to the steady state. A spatially varying time step along with a CFL number of 4 is used to speed convergence to the steady state. Eigenvalue-scaled artificial dissipation and variable-coefficient implicit residual smoothing are used along with a full-multigrid method. The overall accuracy of the code is second order. No wall functions are used, thus avoiding any bias to the complex three-dimensional flow structures near the blade or any other surface.

While the Glenn-HT code has the original k-ω model (Wilcox, 1988), the shear stress transport (SST) model of Menter (1994), and the k-ω model of Wilcox (1998) were implemented in it for comparing the experimental heat transfer data of Giel et al. (1999) on a transonic turbine rotor. The SST model encompasses both the k-ω and the k-ε models, with the original k-ω model of Wilcox (1988) activated in the near-wall region and the standard k-ε model (Jones and Launder, 1973) activated in the outer wake region and in free shear layers. Moreover,

the definition of eddy viscosity is modified to account for the transport of the principal turbulent shear stress. The reader is referred to Menter (1994) for an elucidating discussion of the SST model. Following Menter (1994), the equations for the SST model can be written as

$$\frac{D(\rho k)}{Dt} = \tau_{ij}\frac{\partial u_i}{\partial x_j} - \beta^* \rho \omega k + \frac{\partial}{\partial x_j}\left[(\mu + \sigma_k \mu_t)\frac{\partial k}{\partial x_j}\right] \quad (1)$$

$$\frac{D(\rho \omega)}{Dt} = \frac{\gamma}{\nu_t}\tau_{ij}\frac{\partial u_i}{\partial x_j} - \beta \rho \omega^2 + \frac{\partial}{\partial x_j}\left[(\mu + \sigma_\omega \mu_t)\frac{\partial \omega}{\partial x_j}\right]$$
$$+ 2\rho(1 - F_1)\sigma_{\omega_2}\frac{1}{\omega}\frac{\partial k}{\partial x_j}\frac{\partial \omega}{\partial x_j} \quad (2)$$

where the shear stress is given by

$$\tau_{ij} = \mu_t\left(\frac{\partial u_i}{\partial x_j} + \frac{\partial u_j}{\partial x_i} - \frac{2}{3}\frac{\partial u_k}{\partial x_k}\delta_{ij}\right) - \frac{2}{3}\rho k \delta_{ij} \quad (3)$$

δ_{ij} being the Kronecker delta. Note that the production term in Eqs. (1) or (2) can be written as

$$\tau_{ij}\frac{\partial u_i}{\partial x_j} = \mu_t\left[S_{ij}^2 - \frac{2}{3}\left(\frac{\partial u_k}{\partial x_k}\right)^2\right] - \frac{2}{3}\rho k \frac{\partial u_k}{\partial x_k} \quad (4)$$

where the strain rate tensor is given by

$$S_{ij} = \frac{\partial u_i}{\partial x_j} + \frac{\partial u_j}{\partial x_i} \quad (5)$$

It is known that in aerodynamic applications, use of S^2 in Eq. (4) leads to very high heat transfer coefficient at the leading edge of a blade. To avoid this, use of Ω^2 or $S\Omega$ is recommended (Menter 1992; Kato and Launder 1993), where Ω is the absolute value of the vorticity. These suggestions follow from the fact that for a stagnation flow, $\Omega = 0$ and for a simple shear flow, use of $S\Omega$ is identical to that of S^2. Based upon comparison with experimental data, we recommend the use of $S\Omega$ and will later describe the effect of using S^2, $S\Omega$ or Ω^2 in Eq. (4) on the heat transfer coefficient at the blade surface.

If ϕ_1 represents any constant in the original k-ω model (σ_{k1}, ...), and ϕ_2 any constant in the transformed k-ε model (σ_{k2}, ...), then ϕ, the corresponding constant of the new model given by Eqs. (1) and (2) is

$$\phi = F_1\phi_1 + (1 - F_1)\phi_2 \quad (6)$$

where

$$F_1 = \tanh(arg_1^4)$$
$$arg_1 = \min\left[\max\left(\frac{\sqrt{k}}{0.09\omega y}, \frac{500\nu}{y^2\omega}\right), \frac{4\rho\sigma_{\omega_2}k}{CD_{k\omega}y^2}\right] \quad (7)$$

$$CD_{k\omega} = \max\left(2\rho\sigma_{\omega_2}\frac{1}{\omega}\frac{\partial k}{\partial x_j}\frac{\partial \omega}{\partial x_j}, 10^{-20}\right)$$

y is the distance to the next surface, and $CD_{k\omega}$ is the positive portion

of the cross-diffusion term of Eq. (2). The choice of terms within arg_1 is detailed in Menter (1994). As arg_1 goes to zero near the boundary-layer edge, so does F_1 so that the standard k-ε model is used in that region. For the SST model, the various constants are:

$$\sigma_{k_1} = 0.85, \quad \sigma_{\omega_1} = 0.5, \quad \beta_1 = 0.075, \quad \alpha_1 = 0.31$$
$$\beta^* = 0.09, \quad \kappa = 0.41, \quad \gamma_1 = \beta_1/\beta^* - \sigma_{\omega_1}\kappa^2/\sqrt{\beta^*}$$
$$\sigma_{k_2} = 1.0, \quad \sigma_{\omega_2} = 0.856, \quad \beta_2 = 0.0828$$
$$\gamma_2 = \beta_2/\beta^* - \sigma_{\omega_2}\kappa^2/\sqrt{\beta^*} \quad (8)$$

and the eddy viscosity is defined as

$$\nu_t = \frac{\alpha_1 k}{\max(\alpha_1\omega, \Omega F_2)} \quad (9)$$

where F_2 is given by

$$F_2 = \tanh(arg_2^2), \quad arg_2 = \max\left(2\frac{\sqrt{k}}{0.09\omega y}, \frac{500\nu}{y^2\omega}\right) \quad (10)$$

We may note that Eqs. (7) and (10) require the computation of y, the distance to a wall. This can be complicated for a multi-block grid, such as in the present case. A simple remedy, however, is to set $1/y$ to zero for all grid cells initially, and to compute $1/y$ once only for those blocks that have a wall boundary condition. In fact, if a block has more than one wall, one can specify

$$\frac{1}{y} = \frac{1}{y_1} + \frac{1}{y_2} + \cdots \quad (11)$$

where y_1 is the distance of a grid cell from one wall, y_2 is the distance of the same cell from the second wall, and so on. It is easy to use any other combination in Eq. (11). However, a negligible difference in the heat transfer coefficient on the blade surface was found whether Eq. (11) was used or $1/y$ was taken to be the maximum of $1/y_1$ and $1/y_2$ for a block limited by the blade and the hub. This scheme works since for the SST model, the k-ω model is activated in the near-wall region while the standard k-ε model is activated in the outer wake region and in free shear layers. We realize that this scheme may have some limitations based on how various blocks are configured in the grid.

With $F_1 = 1$, Eqs. (1) and (2) yield the k-ω model where, following Wilcox (1988), the constants are

$$\sigma_{k_1} = 0.5, \quad \sigma_{\omega_1} = 0.5, \quad \beta_1 = 0.075$$
$$\beta^* = 0.09, \quad \gamma_1 = 5/9, \quad \nu_t = k/\omega \quad (12)$$

for Wilcox's 1988 model. For Wilcox's 1998 model, $\beta_1 = 0.072$, $\gamma_1 = 0.52$, and there are a few more modifications (cf. Wilcox, 1998, p. 121). It may be noted that the low-Re version of the Wilcox's k-ω models was used, for which the constants β^* and γ_1 are modified (Wilcox, 1998, p. 198).

It is assumed that the effective viscosity for turbulent flows can be written as

$$\mu_{ef} = \mu_l + \mu_t \tag{13}$$

where the laminar viscosity μ_l is calculated using a power-law for its dependence on temperature (Schlichting, 1979). The turbulent viscosity μ_t is computed using the SST or the low-Re k-ω model described above. The turbulent thermal diffusivity is computed from

$$\alpha_t = \frac{\mu_t}{\rho\, Pr_t} \tag{14}$$

where a constant value of 0.9 is used for the turbulent Prandtl number, Pr_t.

Boundary Conditions

At the main flow inlet boundary located at an axial distance equal to the blade axial chord upstream of the blade leading edge, the total temperature, total pressure, whirl, and meridional flow angle are specified, and the upstream-running Riemann invariant based on the total absolute velocity is calculated at the first interior point and extrapolated to the inlet. The velocity components are then decoupled algebraically, and the density is found from total temperature, total pressure and total velocity using an isentropic relation. For the turbulence model, the value of k and ω is specified using the experimental conditions, namely

$$k = 1.5\,(U_{in} Tu_{in})^2 \,, \qquad \omega = k^{1/2}/\ell \,, \tag{15}$$

where Tu_{in} is the intensity of turbulence at the inlet (taken to be 0.09 or 0.0025 as per experimental data for the rotor), U_{in} is the absolute velocity at inlet, and ℓ is the integral length scale representing the size of the energy containing eddies. This length scale is usually different from that reported as part of the experimental conditions, and needs to be revised as detailed later.

At the main flow exit plane located at an axial distance equal to 80% of the blade axial chord downstream of the blade trailing edge, the static pressure is specified and the density and velocity components are extrapolated from the interior. At the solid surface of the blade and hub, the no-slip condition is enforced, and temperature is specified as per experimental data. The boundary conditions for turbulence quantities on the walls are $k = 0$, and

$$\omega = 100 \left.\frac{\partial u}{\partial y}\right|_{wall} \tag{16}$$

for a hydraulically smooth surface. An upper limit is imposed on the value of ω at the wall, as suggested by Menter (1992) and found effective by Chima (1996),

$$(\omega_{max})_{wall} = \frac{800}{Re}\frac{\nu}{(\Delta y)^2} \tag{17}$$

The grid around the blade extends to mid-way between two adjacent blades with periodic flow conditions in terms of cylindrical velocity components set on a dummy grid line outside this boundary. For a linear cascade (which is true for the experimental data), it is possible to consider only half of the real span for computational purposes with a symmetric boundary condition at mid-span.

Length Scale

The integral length scale describes the average eddy size associated with the turbulence. For flow over a blade, its value affects the passage vortex and thus the heat transfer considerably, as shown later. Moreover, the value of the length scale to be used in computation may differ from that measured experimentally depending upon the definitions used. For the current experimental data (Giel et al., 1999), an auto-correlation yielded a time scale which when multiplied by the mean velocity yielded the integral length scale. If ℓ is the computational length scale defined, as per Wilcox (1998), by

$$\ell(x,y,z,t) = \frac{3}{16} \int_0^\infty \frac{R_{ii}(x,y,z,t;r)}{k(x,y,z,t)}\, dr \tag{18}$$

and ℓ_{exp} is the length scale measured experimentally (Giel et al., 1999) as

$$\ell_{exp}(x,y,z,t) = \frac{1}{2} \int_0^\infty \frac{R_{ii}(x,y,z,t;r)}{k(x,y,z,t)}\, dr \tag{19}$$

then $\ell = (3/8)\,\ell_{exp}$. Here R_{ii} is the auto-correlation tensor for velocity, and dr represents the infinitesimal displacement. We may mention that according to Wilcox (1998), the relation between ω, k and ℓ is given by Eq. (15).

EXPERIMENTAL DETAILS

Measurements were made in a linear cascade facility at the NASA Glenn Research Center (Giel et al., 1999). A turbine blade with 136° of turning, an axial chord of 127 mm and a span of 152.4 mm was tested in a highly three-dimensional flow field resulting from thick inlet boundary layers (cf. Table 1). Data were obtained by a steady-state technique using a heated, isothermal blade. Heat fluxes were determined from a calibrated resistance layer in conjunction with a surface temperature measured by calibrated liquid crystals. Data were obtained for inlet Reynolds numbers of 0.5 and 1.0 × 10^{6}, for isentropic exit Mach numbers of 1.0 and 1.3, and for inlet turbulence intensities of 0.25% and 9.0%. More details are available in Giel et al. (1999).

COMPUTATIONAL DETAILS

The computational span extended from the hub to mid-span of the blade with a symmetric boundary condition at mid-span. In the axial direction, the computational domain extended from the inlet plane located one axial chord upstream of the blade leading edge to the exit plane located 80% of the axial chord downstream of the blade trailing edge. Around the blade, the grid extends to mid-way between two adjacent blades with periodic boundary conditions. Figure 1 shows a spanwise section of the multi-block viscous grid around the blade. The viscous grid is obtained from an inviscid grid by clustering the grid near all the solid walls (blade and hub here). The clustering is done in such a way as to ensure that in the viscous grid, the distance of any cell center adjacent to a solid wall, measured in wall units (y^+), is less than half for the cases studied here, following Boyle and Giel (1992). The average value for this distance was 0.26. The inviscid grid was generated using the commercial code GridPro/az3000 (Program Development Corporation, 1997). For computational accuracy the ratio of two adjacent grid sizes in any direction was kept within 0.8-1.25.

As can be observed from Fig. 1, the grid quality is very good especially near the blade surface.

Initially, the grid consists of 28 blocks but before the solver is used, it can be merged into just 5 blocks using the Method of Weakest Descent (Rigby et al., 1997). The final viscous grid consists of 366080 cells, formed by clustering near the blade and hub from an inviscid grid with 55296 cells. The inviscid grid has 112 cells around the blade (for the O-grid around the blade), 28 cells in the blade-to-blade direction from the blade to the periodic boundary in-between the two blades, and 16 in the spanwise direction. After clustering, the number of cells in the spanwise direction increases to 52 and in the blade-to-blade direction to 60. Three more grids were generated for a grid-independence study. One inviscid grid had 1.5 times the number of cells in each direction as compared to the basic grid described above. Another inviscid grid had 32 cells in the spanwise direction while in the other two directions, the number of cells were the same as in the basic grid. For the third grid, the basic inviscid grid was clustered near the blade and hub with a grid spacing half of that for the basic viscous grid. All these variations of the basic grid yielded nearly the same values for the heat transfer coefficient on the entire blade surface as the basic grid; any variations were within ±2%. The results presented here correspond to the basic grid shown in Fig. 1.

Computations were run on the 16-processor C90 supercomputer at NASA Ames Research Center. The code requires about 40 Mw of storage with all blocks in memory, and takes about 15 s per iteration for two levels of multi-grid. A case requires about 1200 iterations to converge. Both the SST and k-ω (Wilcox, 1998) models take almost the same computational time and display similar numerical stability characteristics. The Wilcox's 1988 k-ω model takes somewhat less time since the constants are simpler than those for the 1998 k-ω model.

RESULTS and DISCUSSION

All the eight experimental cases for the GRC rotor were analyzed for comparison. The values of various parameters for these cases are given in Table 1. Figure 2 shows the static pressure distribution at various spanwise locations on the blade surface for Case 3. While the comparison between the computational and experimental values is very good, we may note that the pressure distribution on the pressure surface is little affected but on the suction surface is strongly affected by the spanwise location. Moreover, the largest adverse pressure gradient regions on the suction surface occur at mid-span, while along the 10% spanwise location, there is almost no adverse pressure gradient region on the suction surface. This may have some effect on the prediction of heat transfer coefficient distribution on the suction surface of the blade by the various turbulence models.

Before discussing the comparison between computed and experimental data for heat transfer, however, let us first resolve the issues about turbulence length scale and use of S^2, Ω^2 or $S\Omega$ in Eq. (4) for the production term. Figure 3 shows the effect of turbulence length scale on the Stanton number distribution on the blade surface using the k-ω model of Wilcox (1998) for $Re_{in} = 1.0 \times 10^6$, $M_{ex} = 0.98$ and $Tu_{in} = 0.09$. The entire blade surface is shown in Fig. 3 with the streamwise distance s measured positive on the suction side starting at the leading edge, and negative on the pressure side of the blade. In this and later figures, both the streamwise distance s and the spanwise distance z from the hub are normalized by the blade span. While

computations are done only over half the span ($0 \le z/\text{span} \le 0.5$), the results are shown for the entire span, and depict clearly that the symmetry boundary condition at mid-span is satisfied. The Stanton number, St, in this and later figures is calculated, as for the experimental data, by

$$St = \frac{-k(\partial T/\partial n)_w}{\rho_{in} U_{in} C_p (T_w - T_{aw})} \qquad (20)$$

where the local adiabatic wall temperature, T_{aw}, is

$$\frac{T_{aw}}{T_{o,in}} = r + \frac{1 - r}{1 + 0.5(\gamma - 1)M_{is}^2} \qquad (21)$$

M_{is} is the local isentropic Mach number, and the recovery factor $r = Pr^{1/3}$ (for turbulent flow) was used. According to Giel et al. (1999), the overall uncertainty in the experimental data for St was determined to be less than 13% in regions where $St < 10^{-3}$, and less than 8% where $St > 2 \times 10^{-3}$. The computed results are shown in Fig. 3 for three values of the turbulence length scale at inlet, namely $\ell = 0.03$, 0.09 and 0.23. While the effect of ℓ on the pressure side of the blade is minor, that on the suction side of the blade is considerable, and stems from its influence on the passage vortex flow, which is essentially a three-dimensional flow phenomenon. As the value of ℓ decreases, the extent of the passage vortex flow increases. This raises the heat transfer coefficient on the entire suction side of the blade, and the effect is quite pronounced in the passage vortex region near the hub. For Wilcox (1988) k-ω model, results are very similar to those in Fig. 3. Differences between the Stanton number contours resulting from the two k-ω models are too small to be displayed here.

The effect of using S^2 or Ω^2 or $S\Omega$ in the production term for Eqs. (1) and (2) is shown in Fig. 4 in terms of the Stanton number distribution on the blade surface. Results are shown for the SST model for Case 1 ($Re_{in} = 10^6$, $M_{ex} = 0.98$, $Tu_{in} = 0.09$ and $\ell = 0.08625$, which corresponds to experimental $\ell = 0.23$). Use of S^2 leads to very high heat transfer coefficient at the leading edge of the blade, as is well known and is shown clearly in Fig. 4(a). This also increases the heat transfer coefficient over the entire blade surface. Use of either Ω^2 or $S\Omega$ leads to small differences in the Stanton number distributions on the blade surface. Comparison of the Stanton number distribution with the experimental data at three spanwise locations, shown in Fig. 5, reveals that use of $S\Omega$ in the production term produces results in closer agreement with the experimental data than that of Ω^2. Thus, $S\Omega$ was used in place of S^2 in Eq. (4) for the results that follow.

Figures 4(c) and 6 show the differences between the SST model and Wilcox (1998) k-ω model in terms of Stanton number distribution on the blade surface for Case 1. While the differences on the pressure surface are minor, those on the leading edge and on the suction surface are appreciable. The SST model yields a bigger passage vortex region near the hub as compared to the k-ω model. This results in higher Stanton number values near the hub but slightly lower values near the mid-span on the suction surface of the blade for the SST model. This is clearly evident from Figs. 5(a) and 7 which provide a comparison with the experimental data at three spanwise locations (10%, 25% and 50%) on the blade for this case. While the computed Stanton number values based on either of the two models compare very well with the

experimental data on the pressure surface, there are discrepancies on the suction surface. The SST model yields a better comparison with the experimental data than the k-ω model at 10% and 25% spanwise locations, while the k-ω model yields a somewhat better comparison at mid-span. This appears to be a direct consequence of two phenomena: 1) a better resolution of the passage vortex region by the SST model, and 2) a better prediction by the k-ω model in large adverse pressure gradient regions. We may recall (cf. Fig. 2) that the largest adverse pressure gradient region lies near mid-span on the suction side of this rotor.

Figure 8 shows the differences between the SST model and Wilcox (1998) k-ω model in terms of Stanton number distribution on the blade surface for Case 3. Here, the SST model yields slightly higher Stanton number values on the pressure surface of the blade, but in contrast to Case 1 in Figs. 4(c) and 6, the k-ω model yields a bigger passage vortex region near the hub as compared to the SST model. This results in higher Stanton number values near the hub but slightly lower values near the mid-span on the suction surface using the k-ω model. This is evident from Fig. 9 which provides a comparison with the experimental data at three spanwise locations (10%, 25% and 50%) on the blade for this case. While the computed Stanton number values based on the SST model compare very well with the experimental data on the pressure surface, those using the k-ω model do not compare that well. The SST model yields a better comparison with the experimental data than the k-ω model at mid-span, while the k-ω model yields a somewhat better comparison at 10% and 25% spanwise locations. These trends (in terms of heat transfer prediction by the SST and k-ω models) are in direct contrast to the observations made above for Case 1. Since the SST model provides a better overall comparison with the experimental data, rest of the cases in Table 1 were run using the SST model only.

Figure 10 provides a comparison with the experimental data for Cases 2 and 4 at three spanwise locations using the SST model. While the Stanton number values compare well on the pressure side of the blade and at the leading edge, there are quantitative differences between the computed and experimental data on the suction side. The qualitative nature of the predictions compares well with the experimental data except that interaction of the shock wave with the boundary layer downstream of the throat (at s/span $\approx$ 1.25) is not predicted by the SST model.

Figure 11 compares the experimental data for Cases 5 and 6 at three spanwise locations with the results computed using the SST model. Again, the comparison is very good on the pressure side of the blade and at the leading edge, but it is not so good on the suction side of the blade. For the transonic Case 6, the SST model does not predict the shock wave downstream of the throat, as for Cases 2 and 4 in Fig. 10.

Figure 12 compares the experimental data for Cases 7 and 8 at three spanwise locations with the results computed using the SST model. Here, the comparison is not good over the entire blade surface, including the leading edge of the blade. Both these cases are for very low turbulence level ($Tu_{in} = 0.0025$), which is not practical in real turbines. Thus, a poor comparison for these cases should not be of much concern. We may also note that the Reynolds number is half of that for cases 3 and 4 discussed earlier for the low turbulence level.

CONCLUSIONS

Two versions of the two-equation k-ω model and a shear stress transport (SST) model are used in a three-dimensional, multi-block, Navier-Stokes code to compare the detailed heat transfer measurements (Giel et al., 1999) on a transonic turbine blade. It is found that the SST model resolves the passage vortex better on the suction side of the blade, thus yielding a better comparison with the experimental data than either of the k-ω models. However, in large adverse pressure gradient regions, such as in the mid-span region on the suction side of this blade, the prediction of heat transfer coefficient by the SST model may be poorer than that by the k-ω model. Moreover, the prediction by any of the turbulence models tested here is still deficient on the suction side of the blade.

Use of the SST model does require the computation of distance from a wall, which for a multi-block grid, such as in the present case, can be complicated. However, a relatively easy fix for this problem was devised. Also, both the k-ω and SST models were found to have similar numerical stability and convergence characteristics. Some issues related to the application of two-equation turbulence models have also been resolved. For example, upon comparison with the experimental data, it is found that for aerodynamic applications use of $S\Omega$ is better than using either S^2 or Ω^2 for the computation of production term in the turbulence equations. Also, the turbulence length scale influences the passage vortex on the suction side of the blade, and thus the relation between the computational and experimental values of the length scale becomes important. For the present study, the two values of the length scale are related via a factor of 3/8.

REFERENCES

Boyle, R.J. and Giel, P., 1992, Three-Dimensional Navier Stokes Heat Transfer Predictions for Turbine Blade Rows, AIAA Paper 92-3068.

Chima, R.V., 1996, A k-ω Turbulence Model for Quasi-Three-Dimensional Turbomachinery Flows, AIAA Paper 96-0248.

Giel, P.W., Van Fossen, G.J., Boyle, R.J., Thurman, D.R. & Civinskas, K.C., 1999, Blade Heat Transfer Measurements and Predictions in a Transonic Turbine Cascade, ASME Paper 99-GT-125.

Jameson, A., Schmidt, W. and Turkel, E., 1981, Numerical Solutions of the Euler Equations by Finite Volume Methods Using Runge-Kutta Time-Stepping Schemes, AIAA Paper 81-1259.

Jones, W.P. and Launder, B.E., 1973, The Calculation of Low-Reynolds-Number Phenomena with a Two Equation Model of Turbulence, *Int. J. Heat Mass Transfer*, vol. 16, pp. 1119-1130.

Kato, M. and Launder, B.E., 1993, The Modelling of Turbulent Flow Around Stationary and Vibrating Square Cylinders, *Proc. 9th Symp. Turbulent Shear Flows*, Kyoto, Japan, 10-4-1.

Menter, F.R., 1992, Improved Two-Equation k-ω Turbulence Models for Aerodynamic Flows, NASA TM 103975.

Menter, F.R., 1994, Two-Equation Eddy-Viscosity Turbulence Models for Engineering Applications, *AIAA J.*, vol. 32, pp. 1598-1605.

Menter, F.R., 1996, A Comparison of Some Recent Eddy-Viscosity Turbulence Models, *J. Fluids Eng.*, vol. 118, pp. 514-519.

Moore, J.G. and Moore, J., 1999, Realizability in Turbulence Modeling for Turbomachinery CFD, ASME Paper 99-GT-24.

Moss, R.W. and Oldfield, M.L.G., 1992, Measurements of the Effect of Free-Stream Turbulence Length Scale on Heat Transfer, ASME Paper 92-GT-244.

Program Development Corporation, 1997, "GridPro™/az3000 - User's Guide and Reference Manual," White Plains, NY.

Rigby, D.L., Steinthorsson, E. and Coirier, W.J., 1997, Automatic Block Merging Using the Method of Weakest Descent, AIAA Paper 97-0197.

Schlichting, H., 1979, *Boundary Layer Theory*, McGraw-Hill, New York, 7th edition, pp. 312-313.

Steinthorsson, E., Ameri, A.A. and Rigby, D.L., 1997, TRAF3D.MB - A Multi-Block Flow Solver for Turbomachinery Flows, AIAA Paper 97-0996.

Van Fossen, G.J., Simoneau, R.J. and Ching, C.Y., 1995, Influence of Turbulence Parameters, Reynolds Number, and Body Shape on Stagnation-Region Heat Transfer, *J. Heat Transfer*, vol. 117, pp. 597-603.

Wilcox, D.C., 1988, Reassessment of the Scale-Determining Equation for Advanced Turbulence Models, *AIAA J.*, vol. 26, pp. 1299-1310.

Wilcox, D.C., 1998, Turbulence Modeling for CFD, DCW Industries, 2nd Edn.

Table 1 Parameter Values
Blade axial chord = 127 mm (5.0 in)
Blade span = 152.4 mm (6.0 in)
Inlet Mach number = 0.38
$T_w/T_{o,in}$ = 1.085 for blade; = 1.0 for hub

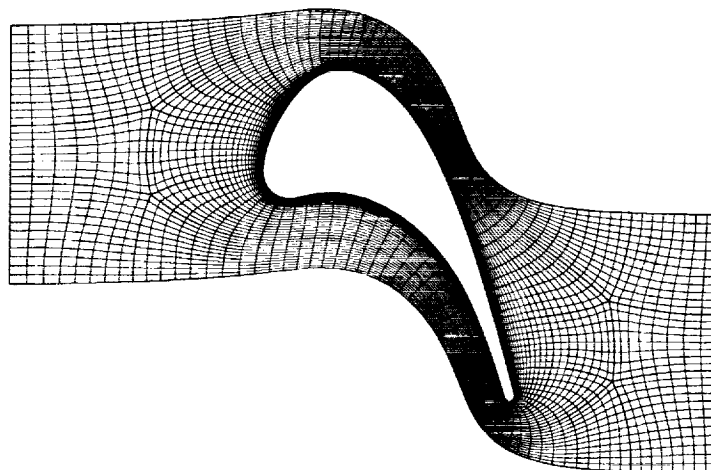| Case	Re_{in}	M_{ex}	Tu_{in}	Exptl. ℓ	Inlet δ
1	1.0×10^6	0.98	0.09	0.23	20.3 mm
2	1.0×10^6	1.32	0.09	0.23	20.3 mm
3	1.0×10^6	0.98	0.0025	0.01	30.5 mm
4	1.0×10^6	1.32	0.0025	0.01	30.5 mm
5	0.5×10^6	0.98	0.09	0.23	20.3 mm
6	0.5×10^6	1.32	0.09	0.23	20.3 mm
7	0.5×10^6	0.98	0.0025	0.01	30.5 mm
8	0.5×10^6	1.32	0.0025	0.01	30.5 mm

Figure 1.-Spanwise section of the multi-block viscous grid around the rotor.
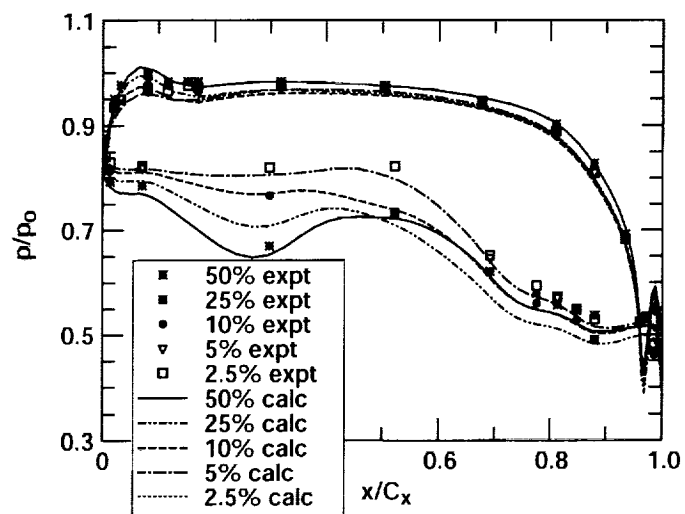

Figure 2.- Static pressure distribution on the blade surface at various spanwise locations for Case 3.
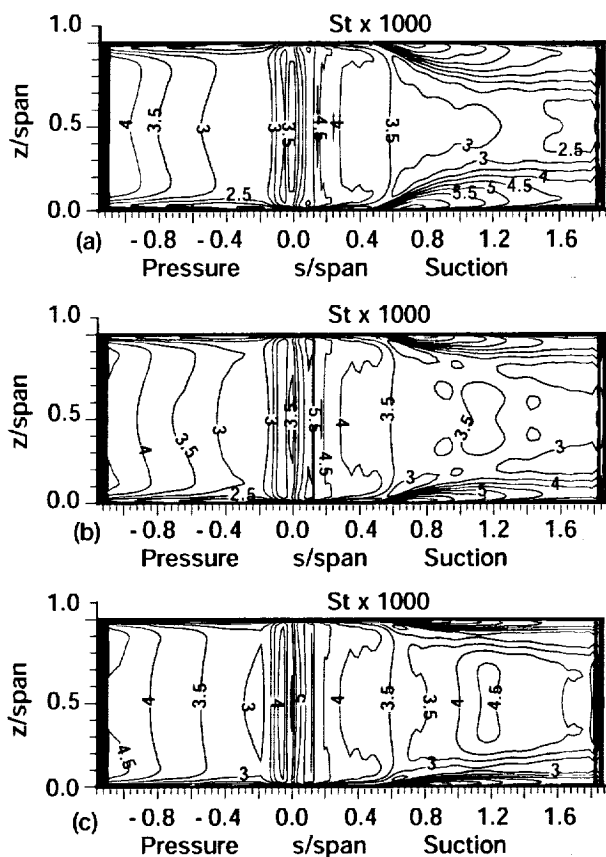
Figure 3.- Effect of turbulence length scale on Stanton
number distribution on the blade using the k- ω model
(1998) for $Re_{in} = 1.0 \times 10^6$; $M_{ex} = 0.98$; $Tu_{in} = 0.09$.
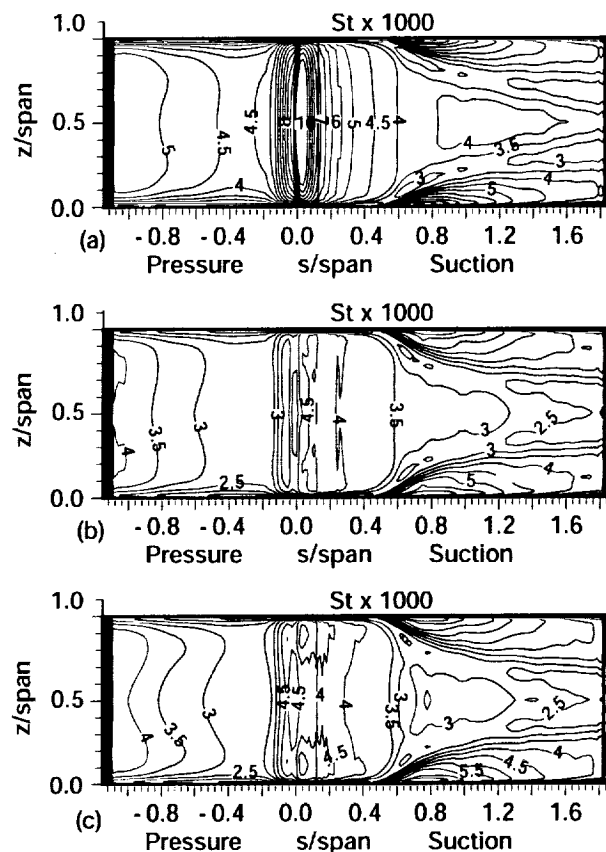(a) Length scale = 0.03. (b) Length scale = 0.09.
(c) Length scale = 0.23.

Figure 4.- Stanton number distribution on the blade using
the SST model for Case 1. (a) with S^2; (b) with V^2; (c) with
SV for production term in Eq. (4).
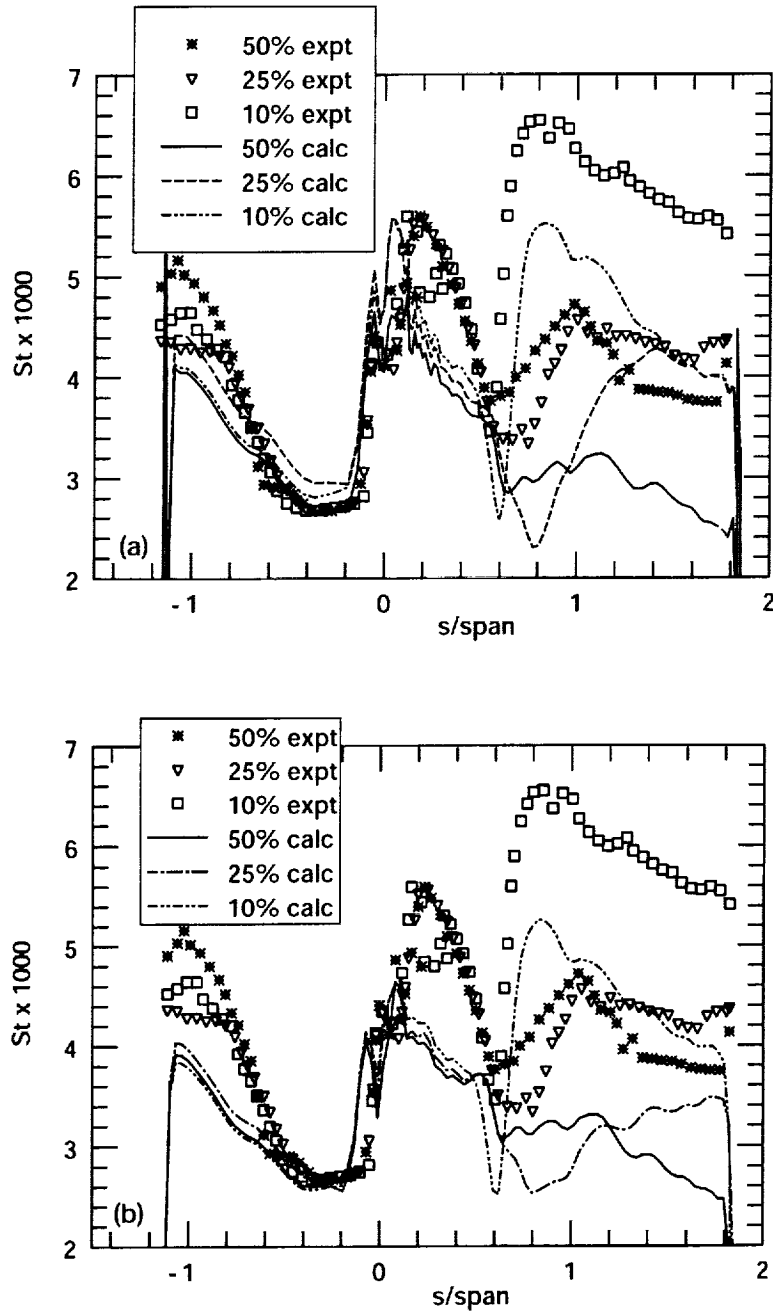
Figure 5.- Comparison with experimental data at three spanwise locations using the SST model for Case 1. (a) with $S\Omega$, (b) with Ω^2 for production term in Eq. (4).

10

St x 1000
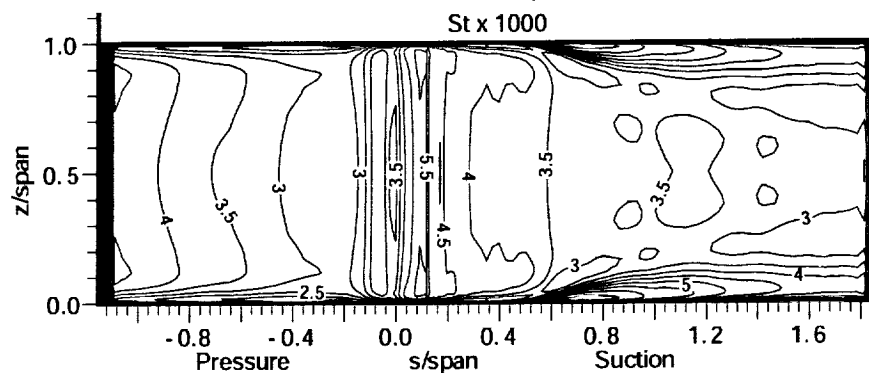
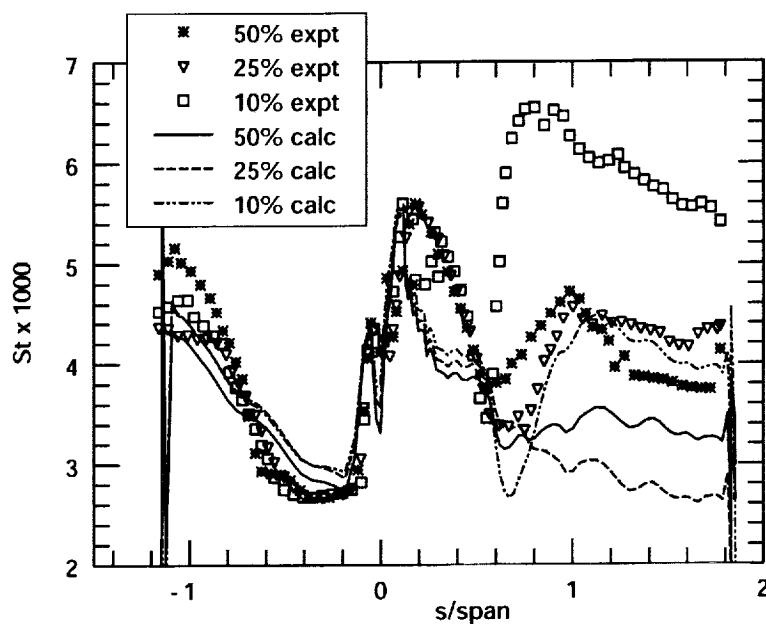Figure 6.- Stanton number distribution on the blade surface for Case 1 using k- ω model (1998).

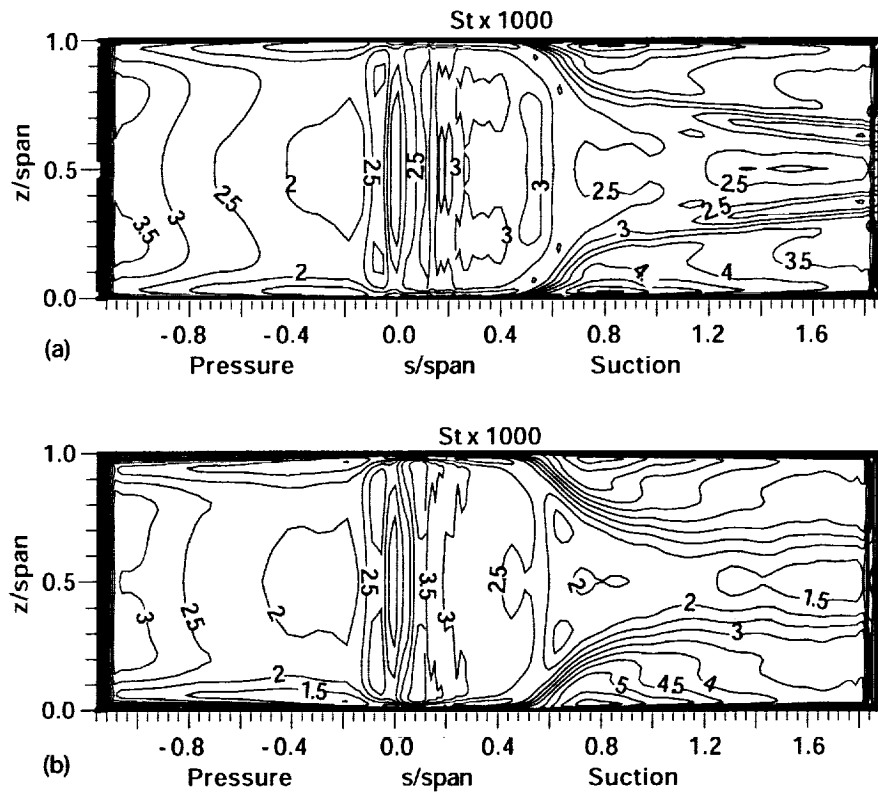Figure 7.- Comparison with experimental data at three spanwise locations using the k- ω model (1998) for Case 1.

Figure 8.- Stanton number distribution on the blade surface for Case 3 using (a) SST model, and (b) k- ω model (1998).

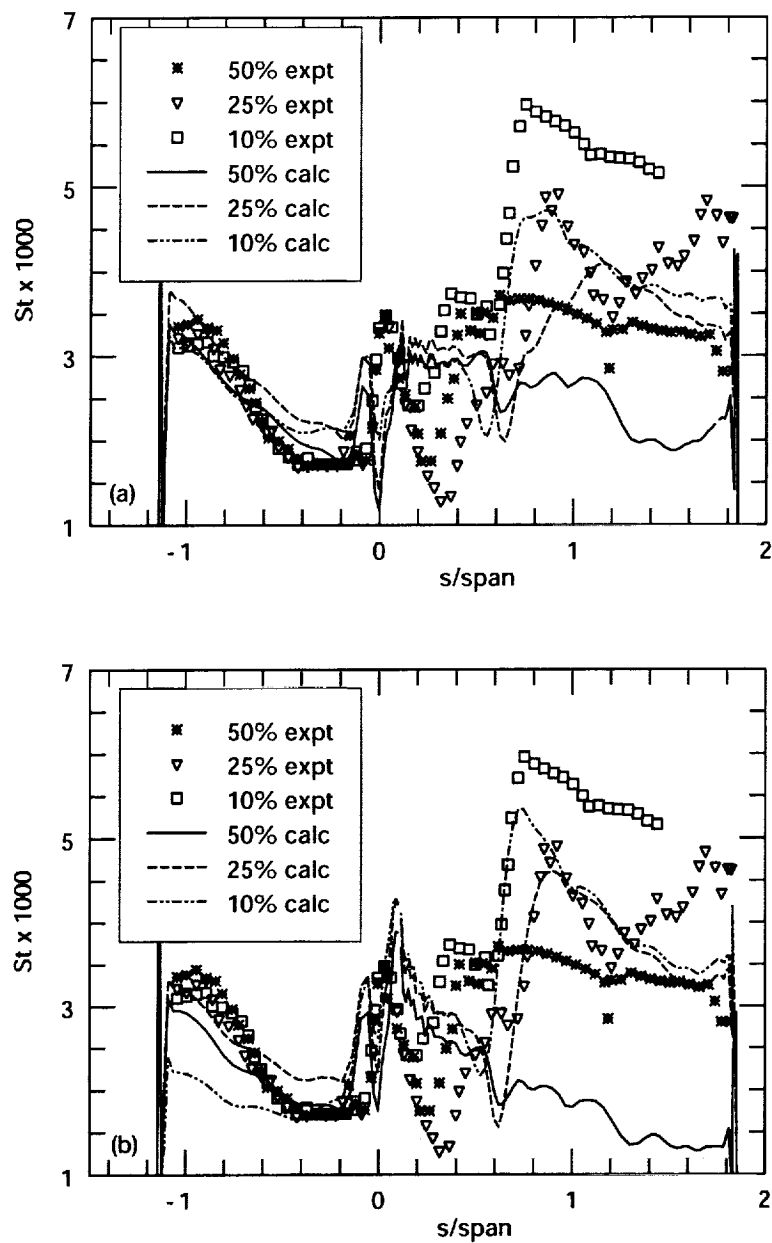Figure 9.- Comparison with experimental data at three spanwise
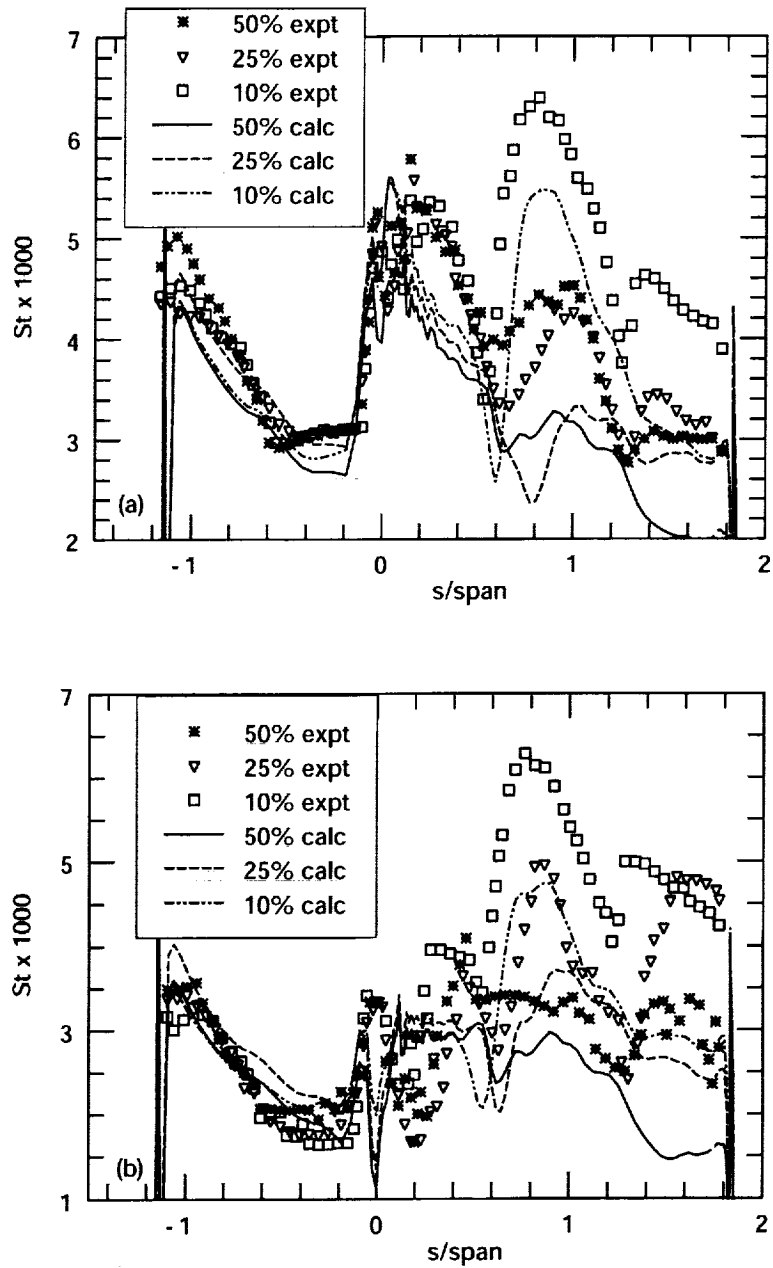locations using (a) SST model, and (b) k- ω model (1998) for Case 3.

Figure 10.- Comparison with experimental data at three spanwise locations using the SST model. (a) Case 2; (b) Case 4.
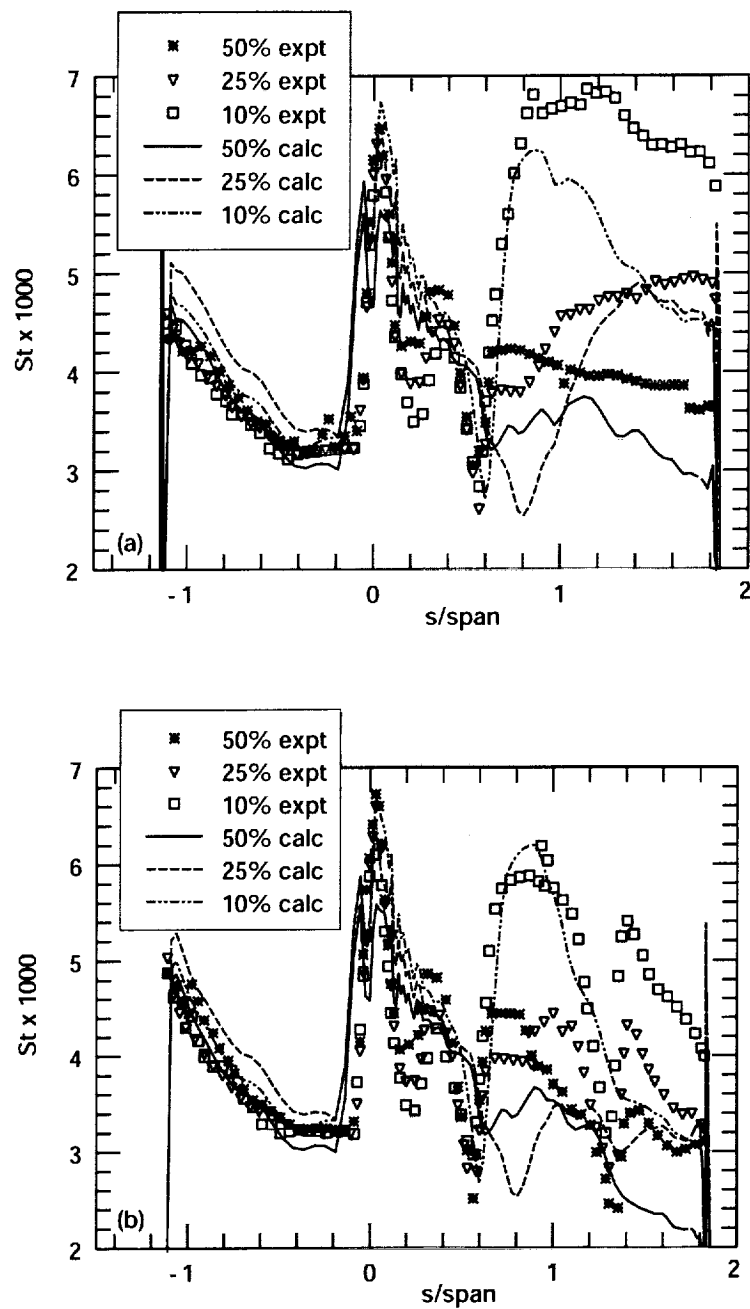
Figure 11.- Comparison with experimental data at three spanwise locations using the SST model. (a) Case 5; (b) Case 6.
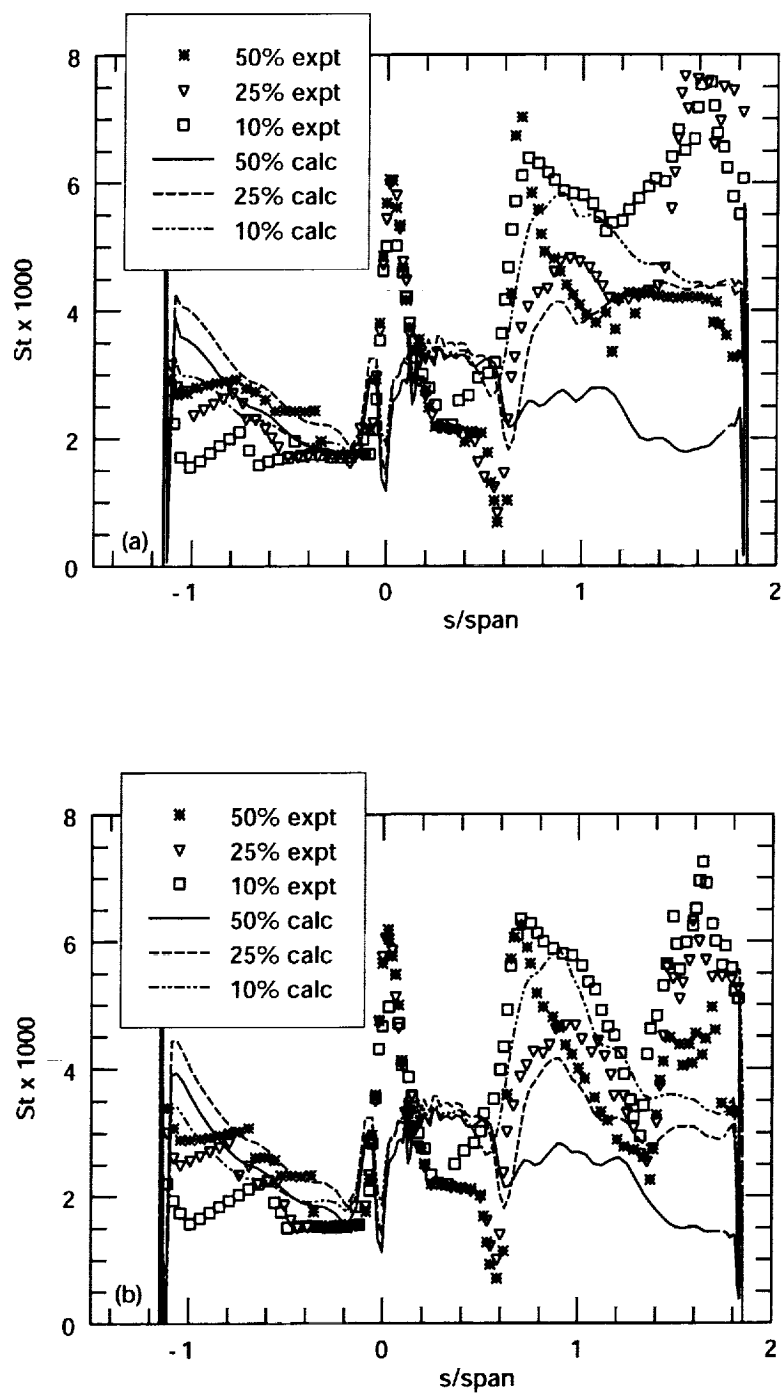
Figure 12.- Comparison with experimental data at three spanwise locations using the SST model. (a) Case 7; (b) Case 8.

REPORT DOCUMENTATION PAGE

Public reporting burden for this collection of information is estimated to average 1 hour per response, including the time for reviewing instructions, searching existing data sources, gathering and maintaining the data needed, and completing and reviewing the collection of information. Send comments regarding this burden estimate or any other aspect of this collection of information, including suggestions for reducing this burden, to Washington Headquarters Services, Directorate for Information Operations and Reports, 1215 Jefferson Davis Highway, Suite 1204, Arlington, VA 22202-4302, and to the Office of Management and Budget, Paperwork Reduction Project (0704-0188), Washington, DC 20503.

1. AGENCY USE ONLY (Leave blank)	2. REPORT DATE	3. REPORT TYPE AND DATES COVERED
	April 2001	Final Contractor Report

4. TITLE AND SUBTITLE

Two-Equation Turbulence Models for Prediction of Heat Transfer on a Transonic Turbine Blade

6. AUTHOR(S)

Vijay K. Garg and Ali A. Ameri

5. FUNDING NUMBERS

WU–714–03–50–00
NAS3–00180

7. PERFORMING ORGANIZATION NAME(S) AND ADDRESS(ES)

AYT Corporation
2001 Aerospace Parkway
Brook Park, Ohio 44142

8. PERFORMING ORGANIZATION REPORT NUMBER

E–12717

9. SPONSORING/MONITORING AGENCY NAME(S) AND ADDRESS(ES)

National Aeronautics and Space Administration
Washington, DC 20546–0001

10. SPONSORING/MONITORING AGENCY REPORT NUMBER

NASA CR—2001-210810
2001–GT–0165

11. SUPPLEMENTARY NOTES

Prepared for the 2001 Turbo Expo sponsored by the American Society of Mechanical Engineers, New Orleans, Louisiana, June 4–7, 2001. Project Manager, R.E. Gaugler, Turbomachinery and Propulsion Systems Division, NASA Glenn Research Center, organization code 5820, 216–433–5882.

12a. DISTRIBUTION/AVAILABILITY STATEMENT

Unclassified - Unlimited
Subject Categories: 34 and 07   Distribution: Nonstandard

Available electronically at http://gltrs.grc.nasa.gov/GLTRS

This publication is available from the NASA Center for AeroSpace Information, 301–621–0390.

12b. DISTRIBUTION CODE

13. ABSTRACT (Maximum 200 words)

Two versions of the two-equation k-ω model and a shear stress transport (SST) model are used in a three-dimensional, multi-block, Navier-Stokes code to compare the detailed heat transfer measurements on a transonic turbine blade. It is found that the SST model resolves the passage vortex better on the suction side of the blade, thus yielding a better comparison with the experimental data than either of the k-ω models. However, the comparison is still deficient on the suction side of the blade. Use of the SST model does require the computation of distance from a wall, which for a multi-block grid, such as in the present case, can be complicated. However, a relatively easy fix for this problem was devised. Also addressed are issues such as (1) computation of the production term in the turbulence equations for aerodynamic applications, and (2) the relation between the computational and experimental values for the turbulence length scale, and its influence on the passage vortex on the suction side of the turbine blade.

14. SUBJECT TERMS

Heat transfer; Turbine; Turbulence modeling

15. NUMBER OF PAGES

22

16. PRICE CODE

A03

17. SECURITY CLASSIFICATION OF REPORT	18. SECURITY CLASSIFICATION OF THIS PAGE	19. SECURITY CLASSIFICATION OF ABSTRACT	20. LIMITATION OF ABSTRACT
Unclassified	Unclassified	Unclassified	

NSN 7540-01-280-5500